

Supporting information for:

**Quantifying Disproportionation in Pharmaceutical Formulations
with ^{35}Cl Solid-State NMR**

David A. Hirsh,¹ Yongchao Su,² Haichen Nei,² Wei Xu,² Dirk Stueber,² Narayan Variankaval,²
and Robert W. Schurko^{1,*}

¹*Dept. of Chemistry & Biochemistry, University of Windsor, Windsor, ON, N9B 3P4, Canada*

²*Merck Research Laboratories, Merck & Co., Inc., Kenilworth, New Jersey 07033, United States*

**Author to whom correspondence should be addressed:*

R.W.S. Phone: 519-253-3000 x3548 E-mail: rschurko@uwindsor.ca

Supporting Information Provided:

	<i>Title</i>	<i>Page</i>
Table S1	$^{35}\text{Cl}\{^1\text{H}\}$ WURST-CPMG experimental NMR parameters	2
Table S2	$^{23}\text{Na}\{^1\text{H}\}$ MAS experimental NMR parameters	3
Table S3	^1H MAS experimental NMR parameters	3
Table S4	^1H - ^{13}C CP/MAS experimental NMR parameters	4
Figure S1	Molecular structures of the compounds in this study	5
Figure S2	Deconvolution of the ^{35}Cl WURST-CPMG NMR spectrum of NaSt_X	5
Figure S3	^{35}Cl Hahn echo NMR spectra of the NaSt -containing samples	6
Figure S4	^{35}Cl NMR spectra of NaSt_X , NaCl(s) , and NaCl(aq) samples	6
Figure S5	^1H - ^{13}C CP/MAS NMR spectra of the NaSt -containing samples	7
Figure S6	PXRD patterns of the NaSt -containing samples	7
Figure S7	^1H - ^{13}C CP/MAS NMR spectra of the MgSt -containing samples	8
Figure S8	PXRD patterns of the MgSt -containing samples	8
Figure S9	^{23}Na MAS NMR spectra of NaSt_X , NaCl(s) , and NaCl(aq) samples	9
Figure S10	Deconvolution of the ^{35}Cl WURST-CPMG NMR spectrum of MgSt_X	9
Figure S11	^1H NMR spectra of MgSt_X and MgSt_XH	10
Figure S12	^{35}Cl Hahn echo NMR spectra of MgSt_X and MgSt_XH	10
Figure S13	^{35}Cl NMR spectra of MgSt_X , $\text{MgCl}_2 \cdot 6\text{H}_2\text{O(s)}$, and $\text{MgCl}_2\text{(aq)}$ samples	11
Figure S14	Effects of processing parameters on quantification of ^{35}Cl SSNMR spectra	11

Table S1. Acquisition parameters for $^{35}\text{Cl}\{^1\text{H}\}$ WURST-CPMG experiments on the **PiogHCl** samples under static sample conditions.

	All Samples
Number of scans	14400
Experimental time (h)	4
Recycle delay (s)	1
Spectral Width (MHz)	1
^{35}Cl WURST pulse width (μs)	25
^{35}Cl WURST pulse rf (kHz)	20.3
^1H decoupling field (kHz)	61.5
Sweep range of WURST pulses (kHz)	500
Points in WURST shape [N]	500
Meiboom-Gill loops [N] (<i>i.e.</i> , Number of echoes)	122
Length of echoes (μs)	125
Acquisition length (number of points)	53250

Table S2. Acquisition parameters for $^{23}\text{Na}\{^1\text{H}\}$ MAS ($\nu_{\text{rot}} = 12$ kHz) Hahn echo experiments on the mixed samples containing **NaSt**.

	All samples
Number of scans	2048
Experimental time (min)	34.1
Recycle delay (s)	1
^{23}Na 90° (CT-selective) pulse width [$\pi/2$] (μs)	1.25
Inter-pulse delay [τ] (us)	83.3
^{23}Na 180° (CT-selective) pulse width [π] (μs)	2.5
^{23}Na rf field (kHz)	100
^1H rf decoupling strength (kHz)	67.4
Spectral width (kHz)	50
Acquisition length (# of points)	4096

Table S3. Acquisition parameters for ^1H MAS ($\nu_{\text{rot}} = 12$ kHz) echo experiments on the **PiogHCl** and stearate-containing samples.

	All Samples
Number of scans	16
Experimental time (min)	5.3
Recycle delay (s)	20
^1H 90° pulse width [$\pi/2$] (μs)	2.5
Inter-pulse delay [τ] (μs)	83.3
^1H 180° pulse width [π] (μs)	5
^1H rf field (kHz)	100
Spectral width (kHz)	100
Acquisition length (# of points)	4096

Table S4. Acquisition parameters for ^1H - ^{13}C CP/MAS ($\nu_{\text{rot}} = 12$ kHz) experiments on the **PiogHCl** and stearate-containing samples.

	All Samples
Number of scans	2880
Experimental time (hrs)	4
Recycle delay (s)	5
^1H 90° pulse width [$\pi/2$] (μs)	2.5
Contact time (ms)	2
^1H rf field during contact pulse (kHz)	43
^{13}C rf field during contact pulse (kHz)	48
^1H decoupling field (kHz)	47
Spectral width (kHz)	59.5
Acquisition length (number of points)	4096

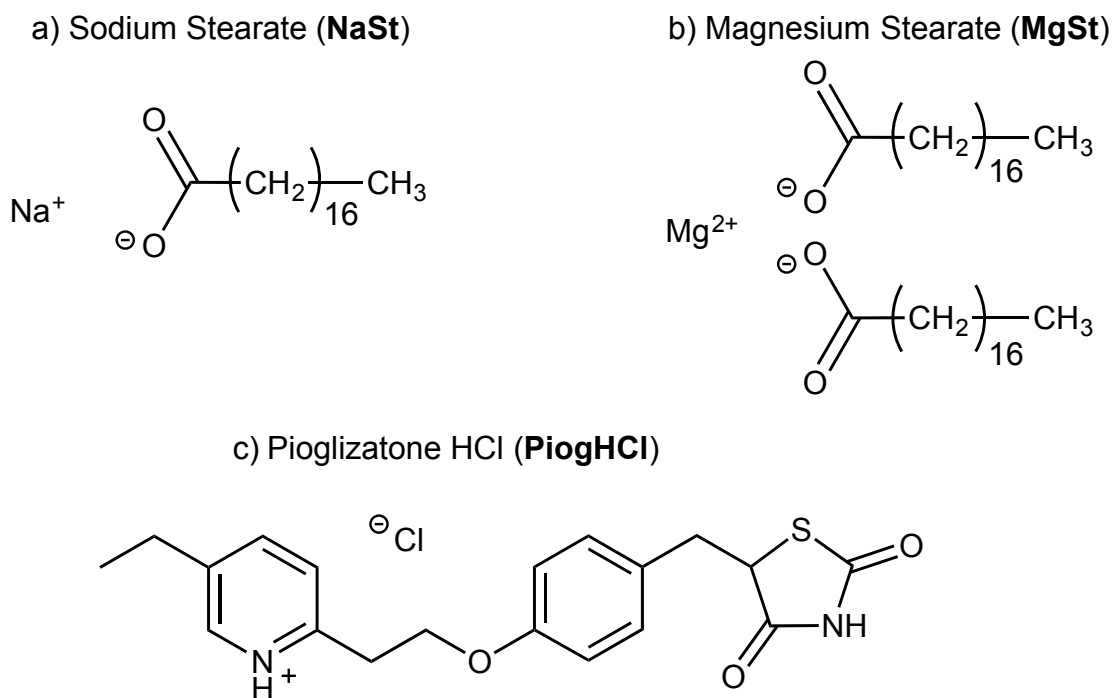


Figure S1. Molecular structures of the compounds used in this study.

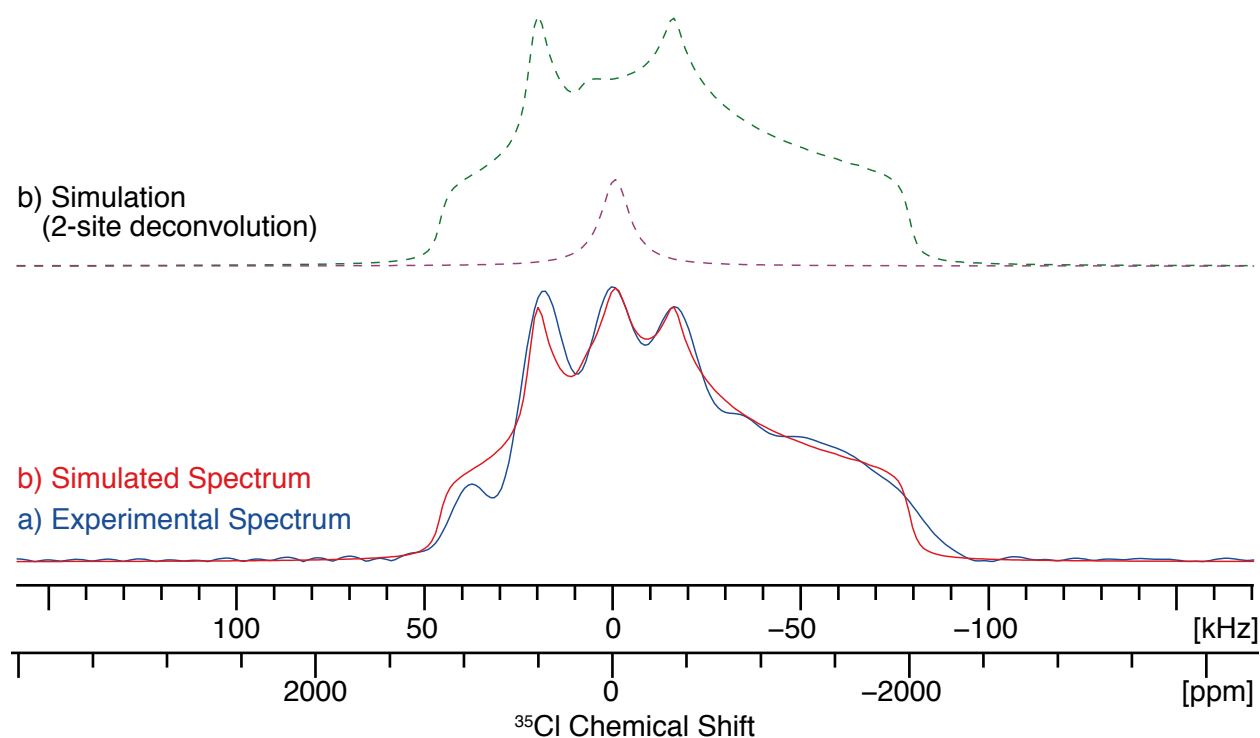
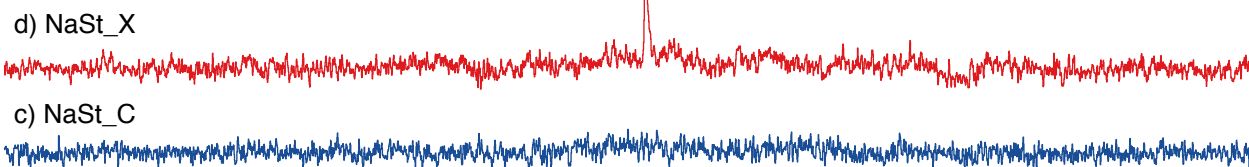


Figure S2. a) Experimental $^{35}\text{Cl}\{^1\text{H}\}$ WURST-CPMG NMR spectrum of **NaSt_X**, and b) the corresponding analytical simulation of the pattern constructed with the 2 subspectra shown in c). The broader site (green dashed line) was created with the parameters from the ^{35}Cl NMR spectrum of pure **PiogHCl**.

**$^{35}\text{Cl}\{^1\text{H}\}$ Hahn Echo
(w/ nonselective pulses)**



$^{35}\text{Cl}\{^1\text{H}\}$ WCPMG

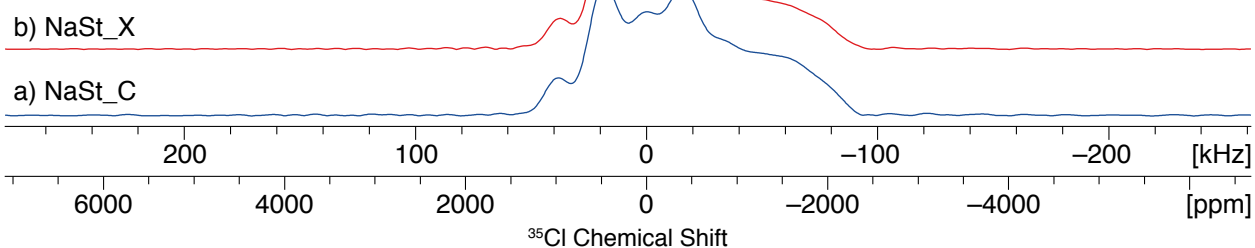


Figure S3. $^{35}\text{Cl}\{^1\text{H}\}$ NMR spectra of the **NaSt**-containing sample mixtures, a) and c) **NaSt_C**, b) and d) **NaSt_X**. The spectra at the bottom were acquired with WURST-CPMG, the spectra at the top were acquired with a Hahn echo sequence using nonselective pulses.

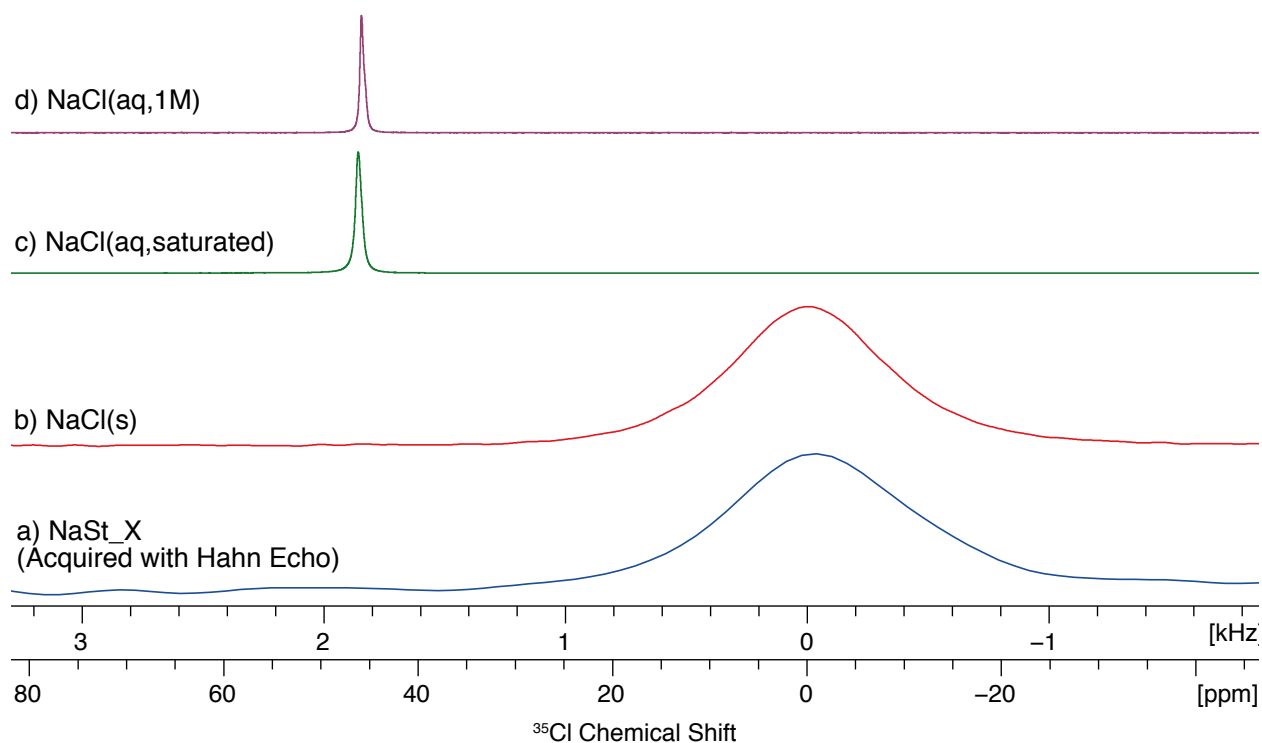


Figure S4. $^{35}\text{Cl}\{^1\text{H}\}$ Hahn echo NMR spectra of a) **NaSt_X**, b) solid NaCl, c) saturated NaCl solution in H_2O , and d) 1 M NaCl solution in H_2O . The spectrum of **NaSt_X** is the same as that in **Figure S3d**.

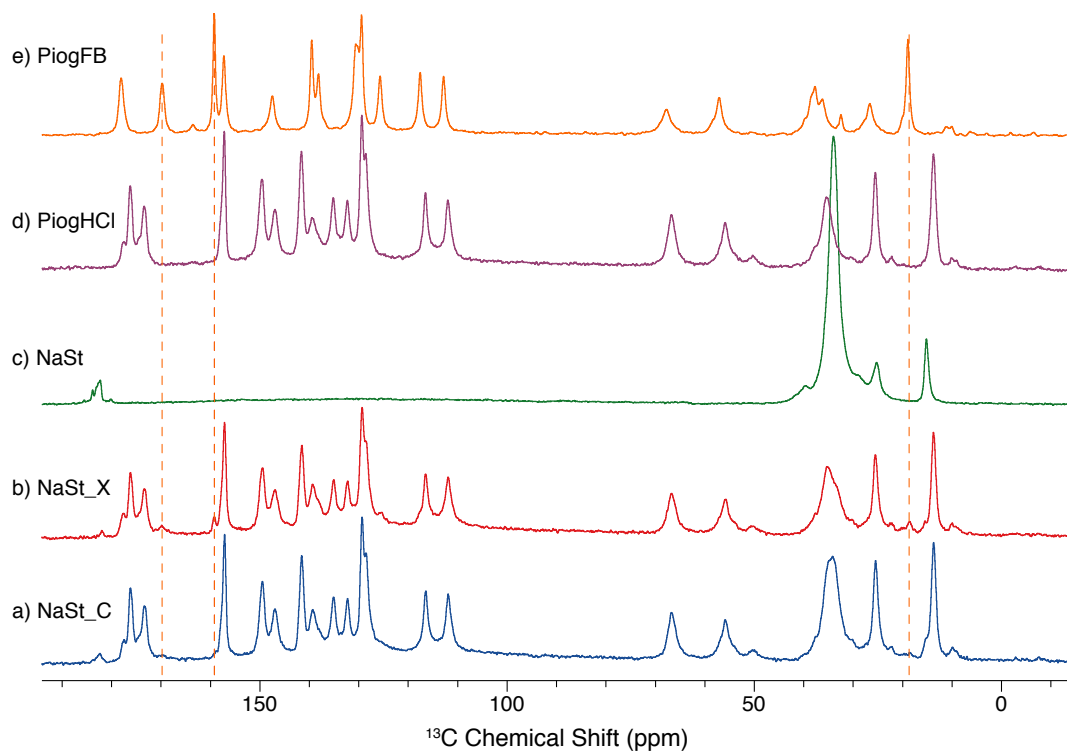


Figure S5. ^1H - ^{13}C CP/MAS ($\nu_{\text{rot}} = 12$ kHz) NMR spectra of the **NaSt**-containing mixed samples and related materials. Dashed lines indicate distinct peaks from **PiogFB** that appear in the spectrum of **NaSt_X** (but not **NaSt_C**).

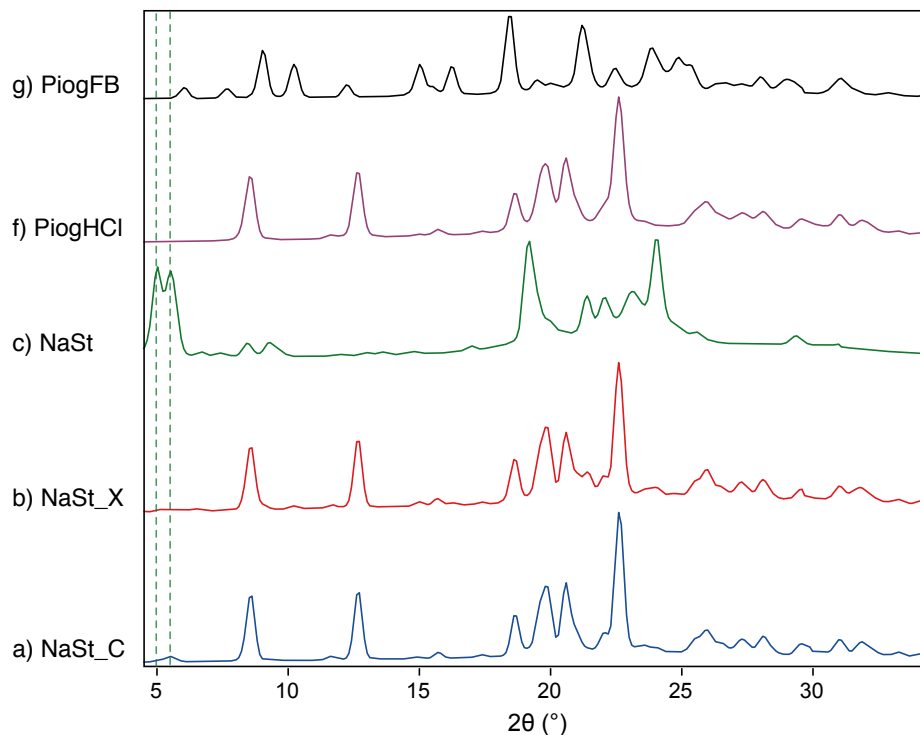


Figure S6. Experimental PXRD patterns of the **NaSt**-containing samples and pure constituents. Dashed lines indicate distinct features from the stearate that are present in the diffraction pattern of **NaSt_C**.

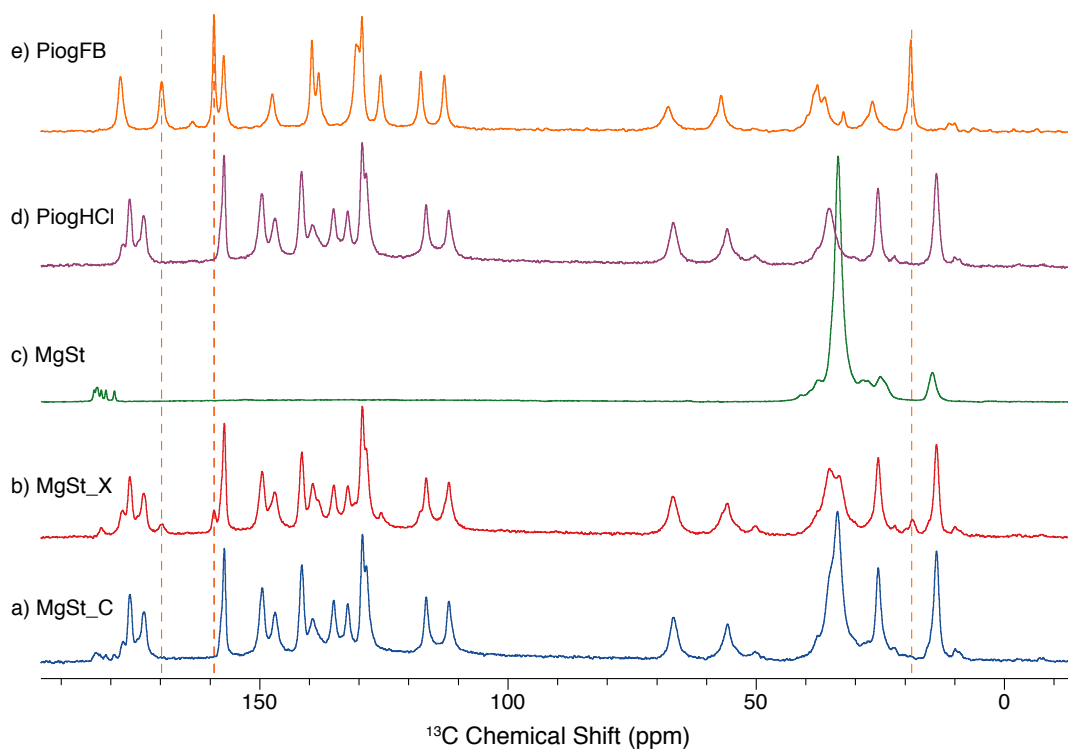


Figure S7. ^1H - ^{13}C CP/MAS ($\nu_{\text{rot}} = 12$ kHz) NMR spectra of the **MgSt**-containing mixed samples and related materials. Dashed lines indicate distinct peaks from **PiogFB** that appear in the spectrum of **MgSt_X** (but not **MgSt_C**).

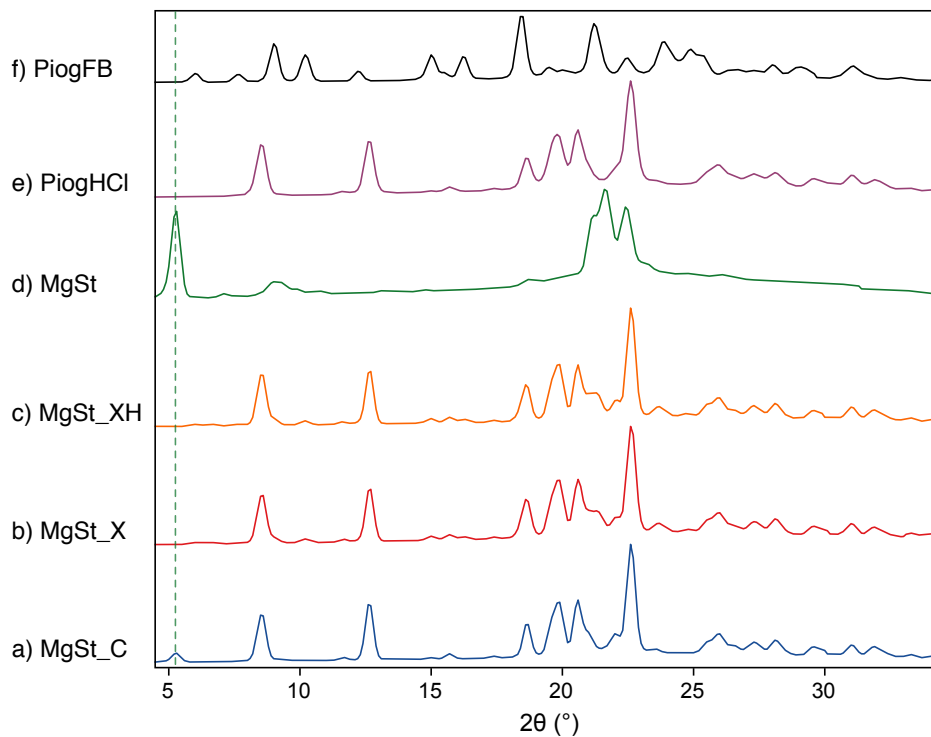


Figure S8. Experimental PXRD patterns of the **MgSt**-containing samples and pure constituents. Dashed lines indicate distinct features from the stearate that are present in the diffraction pattern of **MgSt_C**.

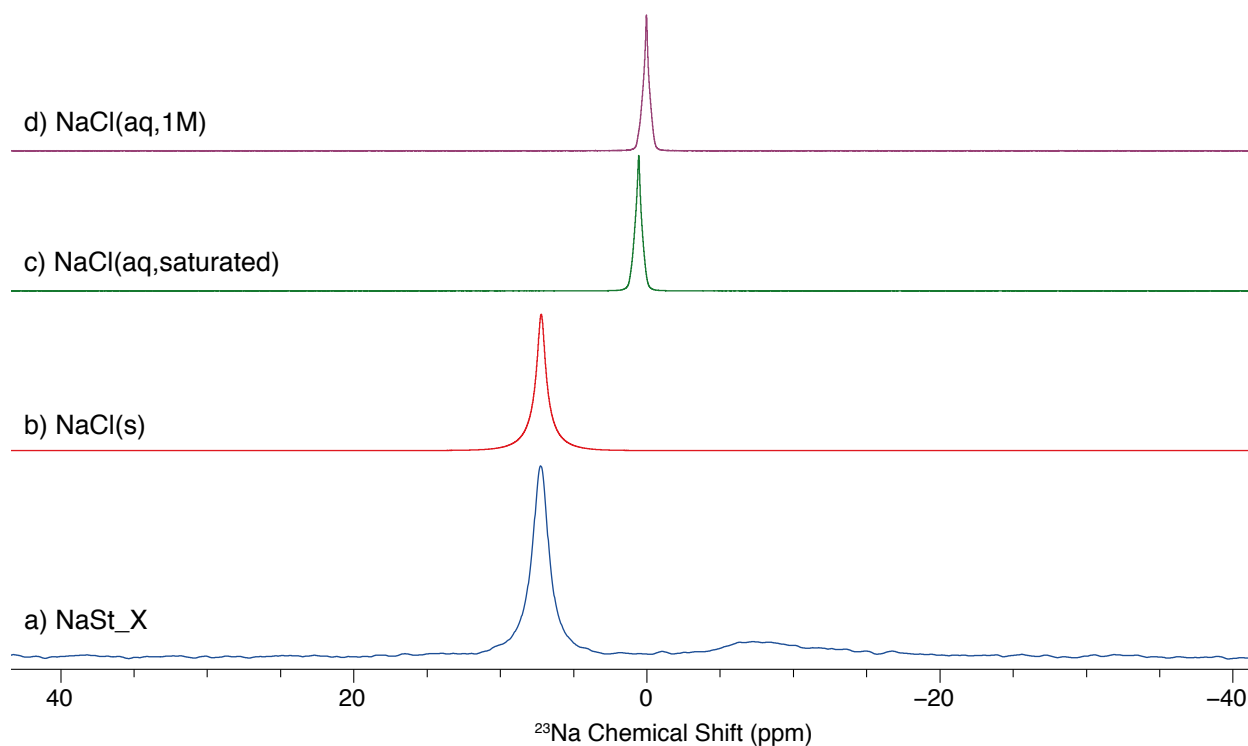


Figure S9. ^{23}Na Hahn echo NMR spectra of a) **NaSt_X**, b) solid NaCl, c) a saturated NaCl solution in H_2O , and d) a 1 M NaCl solution in H_2O . Spectra of the solid samples were acquired with MAS ($\nu_{\text{rot}} = 12$ kHz). The spectrum of **NaSt_X** is the same as that in **Figure 3b**.

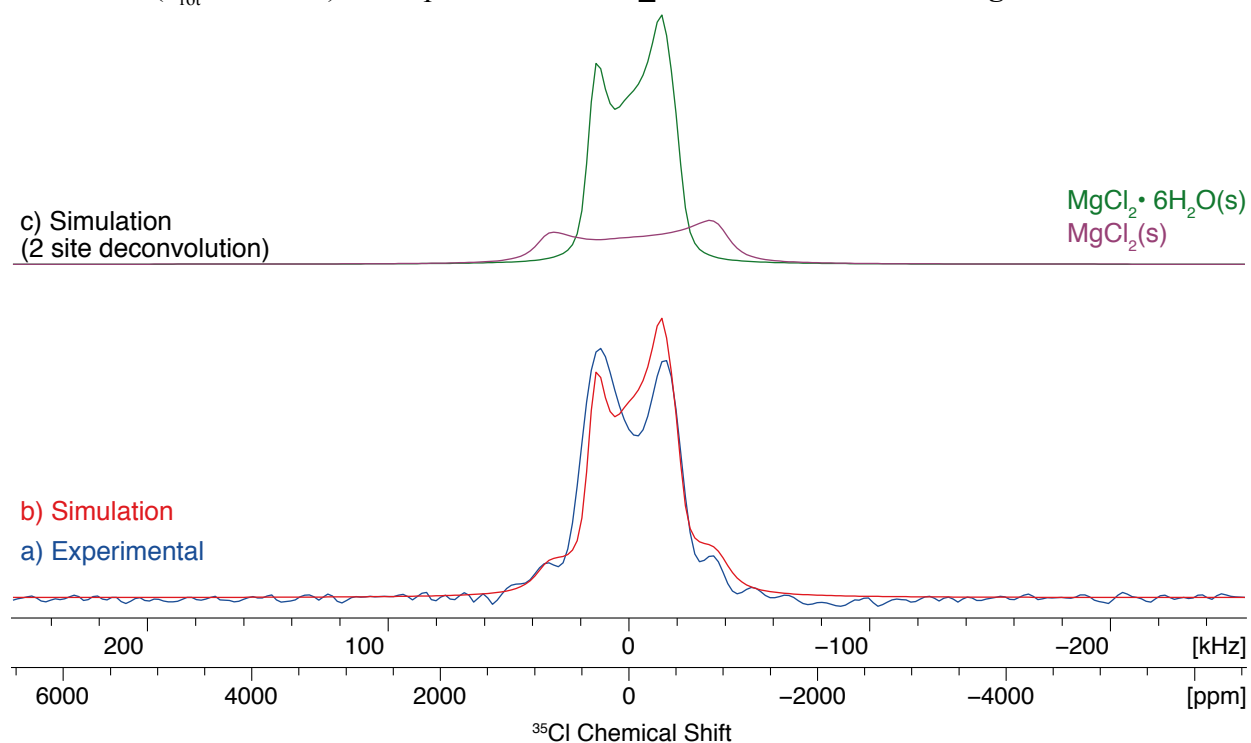


Figure S10. a) Experimental ^{35}Cl WURST-CPMG NMR spectrum of the disproportionation product in the **MgSt_X** sample (obtained by subtracting the signal in the spectrum of **MgSt_C** from that of **MgSt_X**), b) analytical simulation of the pattern constructed with the 2 subspectra shown in c).

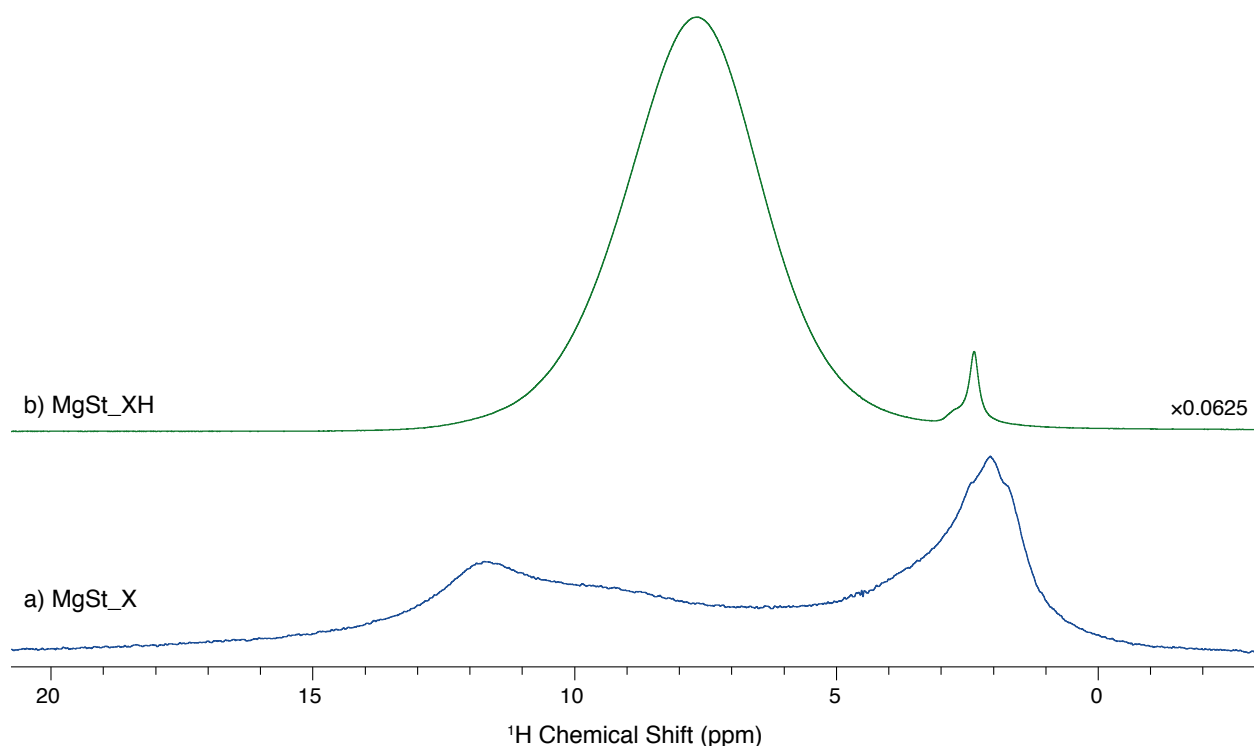


Figure S11. ^1H NMR spectra acquired under static sample conditions of a) **MgSt_X**, and b) **MgSt_XH**, which was prepared by placing 300 mg of **MgSt_X** in a 75% RH chamber for 4 hours.

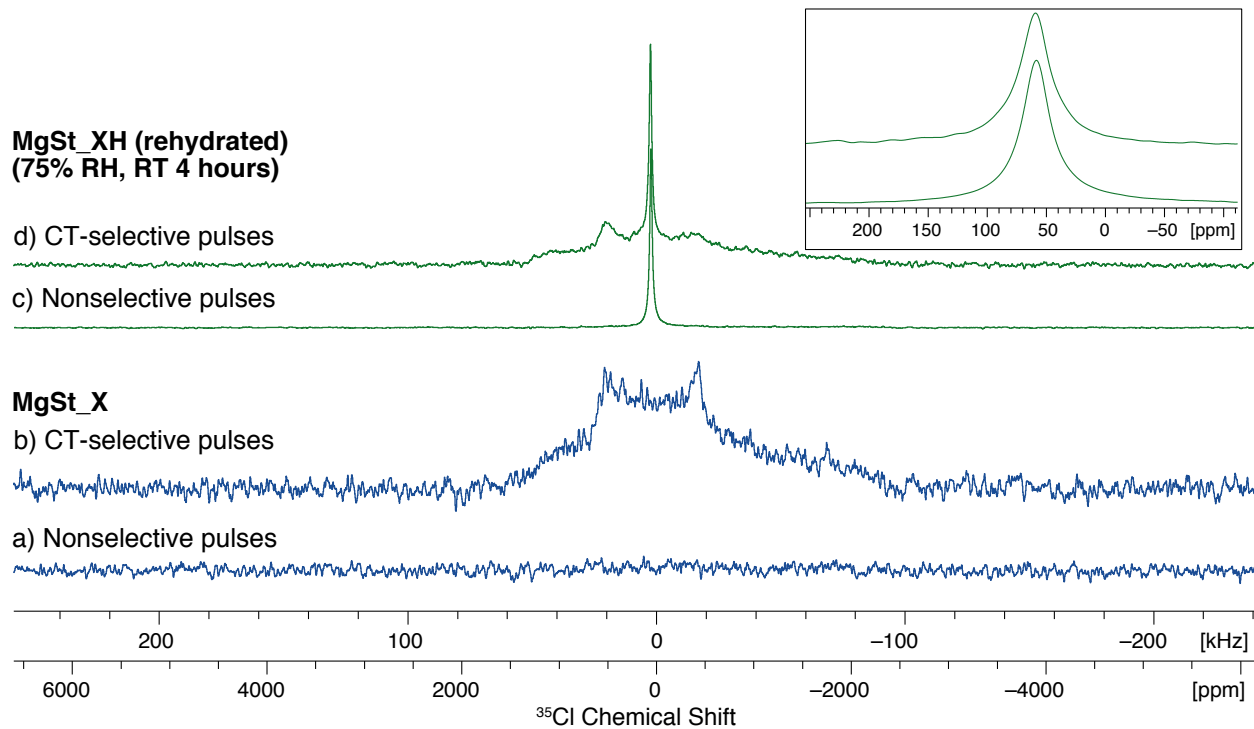


Figure S12. ^{35}Cl Hahn echo NMR spectra of **MgSt_X** (bottom, blue) and **MgSt_XH** (top, green) acquired with nonselective pulses, a) and c), or CT-selective pulses, b) and d). The inset shows an expansion of the region containing the sharp features in the spectra of **MgSt_XH**.

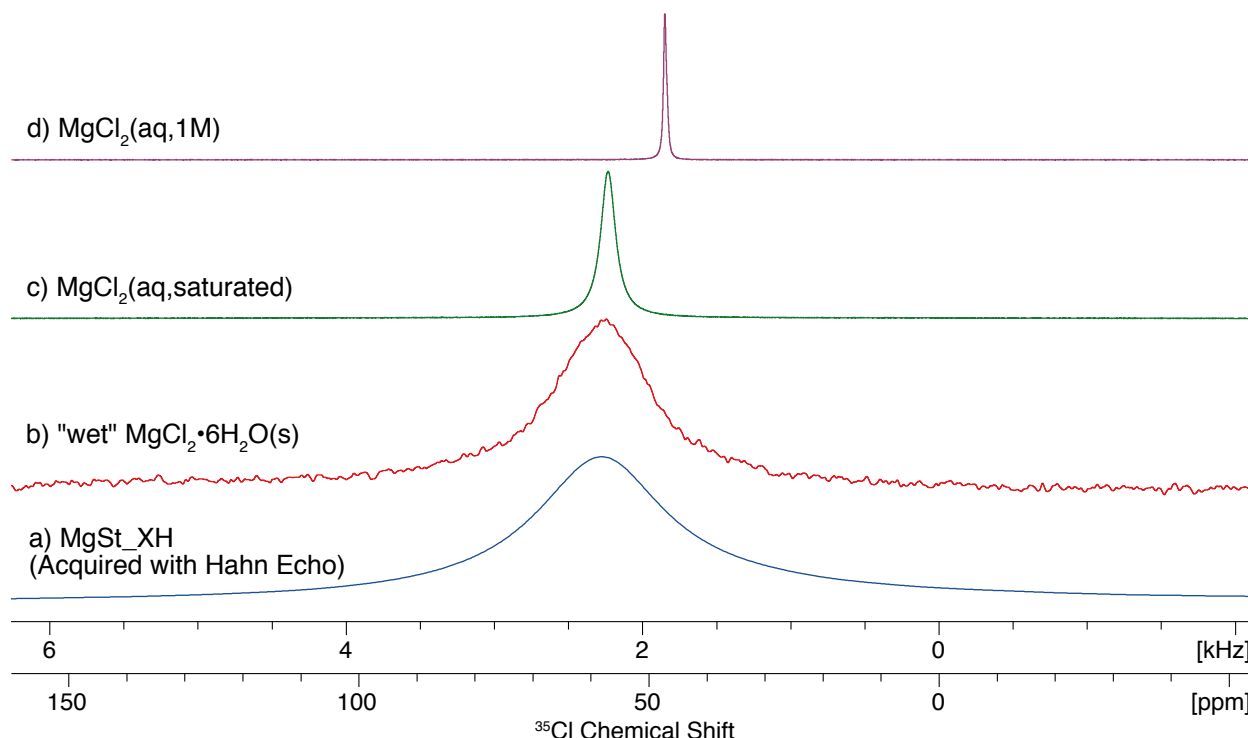


Figure S13. $^{35}\text{Cl}\{^1\text{H}\}$ Hahn echo NMR spectra of a) **MgSt_XH**, b) solid $\text{MgCl}_2 \cdot 6\text{H}_2\text{O}$ that was exposed to moisture in the air, c) saturated MgCl_2 solution in H_2O , and d) 1 M MgCl_2 solution in H_2O . The spectrum of **MgSt_XH** is the same as that in **Figure S12c**.

Effects of Processing Parameters on Quantification of ^{35}Cl SSNMR Spectra

The following discussion pertains to the PiogHCl 90% sample, but the results are consistent for all of the standardization samples. **Figures S14a** and **S14b** show the results of the quantification analysis for all of the spikelets in spectra processed using a total of four different processing methods. These four data sets were prepared from the same experimental data, using combinations of 100 Hz of exponential line broadening (or no line broadening), and by taking the absolute magnitude of the spectrum (or phasing). In the plots, a solid horizontal black line indicates the amount of PiogHCl that is expected to be in the sample based on the sample's preparation (*i.e.*, sample masses of the constituents). Each point in the coloured lines corresponds to a measured value based on the intensity of a given spikelet. As such, the closer a point is to the black line, the higher the accuracy of the measurement.

For measurements using maximum spikelet intensity (**MSI**, **Figure S14a**), spectra processed without line broadening (solid green and open purple squares) produce nearly identical

results, and both have poor accuracy (*i.e.*, all of the values are 10-20 wt-% higher than the expected value). However, with the addition of 100 Hz of line broadening, nearly all of the points move within 5 wt-% of the ideal value, due to increased S/N. Additional line broadening was tested, but produced the same results as 100 Hz and did not lead to improvements in the accuracy. For all of the processing methods, there are a few points at the left and right side of the spectrum that provide inaccurate measurements, regardless of the processing method. Measurements using these points are likely hindered by the low signal at these frequencies due to the inherent shapes of the second-order powder patterns (*cf.* spectrum in **Figure S14c**).

For measurements using the integrated intensities of the spikelets (**ISI**, **Figure S14b**), the only method with poor accuracy is magnitude processing without line broadening (solid green squares). However, when 100 Hz of exponential line broadening are applied prior to Fourier transformation and magnitude calculation,

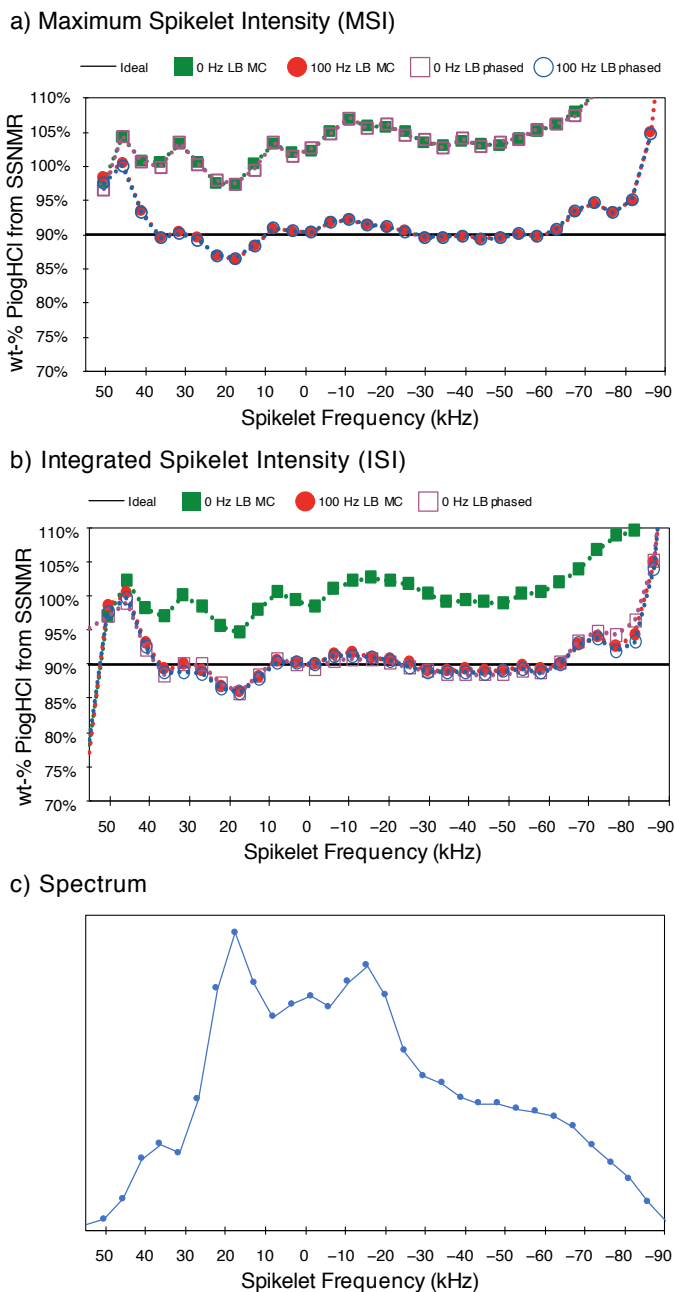


Figure S14. Results of the quantification analysis of the ^{35}Cl NMR spikelet spectrum of PiogHCl 90% using different processing parameters. Intensities were measured using a) spikelet intensities and b) integrated intensities of the spectrum, depicted in c). In a) and b), data were obtained from spectra processed by taking the absolute magnitude (closed shapes) or phasing (open shapes), with (squares) and without (circles) the application of 100 Hz of exponential line broadening.

the results are just as accurate as those obtained when phasing the spectra, and are close to the expected value. Unlike the previous case using peak intensity measurements, if the spectrum is phased, differences in line broadening do not affect the accuracy.

Interestingly, the accuracy of the measurement does not seem to be correlated with the relative intensity of the spikelet as long as the signal is above some minimum threshold. For example, the highest intensity spikelets (known as the “horns”) perform about as well as other parts of the pattern. As mentioned above, points at the two ends of the spectrum (where the pattern has lowest signal intensity) do not perform well, regardless of the processing method used.

The origins of these differences in accuracy are unclear at the moment. We speculate that the importance of line broadening stems from a need to ensure that the echo train has decayed by the end of the acquisition period for accurate quantification. PiogHCl has a long T_2^{eff} , and it is possible that measurements on samples with shorter T_2^{eff} will not be as influenced by line broadening. Additionally, there may be other processing methods that may affect the measurement accuracy, or other factors of the experimental setup that may play a role (*e.g.*, parameters in the swept WURST pulses). Such issues should be tackled with a theoretical approach that is outside the scope of the current proof-of-concept work.

In conclusion, for the PiogHCl system, we observe empirically that 100 Hz line broadening improves the measured values, and that taking the absolute magnitude of the spectra (rather than phasing) is sufficient.